

Geomagnetic Disturbance Effects on Satellite Attitude Estimation

Demet Cilden-Guler^{1*}, Zerefsan Kaymaz², Chingiz Hajiyev³

Faculty of Aeronautics and Astronautics, Istanbul Technical University, Maslak, 34469,
Istanbul, Turkey

¹cilden@itu.edu.tr, ²zerefsan@itu.edu.tr, ³cingiz@itu.edu.tr

Abstract: This study investigates the effects of magnetic disturbances resulting from geospace storms on the satellite attitudes estimated by EKF. It is shown that the increasing levels of geomagnetic activity affect geomagnetic field vectors predicted by IGRF and T89 models. Various sensor combinations including magnetometer, gyroscope, and sun sensor are evaluated for magnetically quiet and active conditions. Errors are calculated for estimated attitude angles and differences were discussed. This study emphasizes on the importance of environmental factors on the satellite attitude determination systems.

Keywords: magnetic field disturbance, IGRF, T89, attitude estimation, sensor fusion, Kalman filtering.

1. Introduction

The orientation of the geomagnetic field is one of the most critical data in determination and control of the satellite's attitude especially at the low Earth orbits (LEO) [1–4]. More accurate measurements of the geomagnetic field lead more accurate predictions of the satellite attitude. Geomagnetic field may be obtained from: 1. In-situ measurements of an on-board spacecraft magnetometer, 2. empirical models of the geomagnetic field that utilize the large amount of spacecraft data, and 3. the simulated magnetometer. Simulated magnetometers are constructed on the ground before the satellite launch to reproduce the satellite magnetometer measurements of real space. In other words, a simulated magnetometer is an object simulated by software for

* Corresponding Author

obtaining the geomagnetic field used to estimate the satellite's attitude. In order to design a simulated magnetometer, a geomagnetic field model, the statistical characteristics of the magnetic field measurements in space and characteristics of on-board satellite magnetometers are needed. The most commonly used geomagnetic field model to predict the Earth's magnetic field at the satellite location is the International Geomagnetic Reference Field (IGRF) model [5,6]. However, the angle between the magnetic field vector from the IGRF model and the magnetic field vector from the simulated magnetometer affects the accuracy of the attitude angles, namely roll, yaw, and pitch. When transformed the vectors into the same coordinates, the smaller this angle is the more precisely the attitude angles are determined. Therefore, the choice of geomagnetic field model used in the simulated magnetometer is very important in achieving high accuracy in attitude angles.

The main source of the geomagnetic field is the Earth's dynamo in its core that produces dipolar magnetic fields in near-Earth space environment [7–9]. However, solar activities such as solar wind, Coronal Mass Ejections (CMEs), high speed streams (HSS), Interplanetary Shocks (IS) and their magnetospheric consequences geomagnetic storms and magnetospheric substorms produce disturbances superimposed on the dipole field of the Earth different strengths [10]. Charged particles from the geomagnetic tail flow into the upper atmosphere and drive electrical currents at the LEO altitudes which in turn modify the geomagnetic field at those altitudes [11–13]. We will refer to the variations caused by these or external sources as magnetic disturbances or magnetic anomalies. While on-board spacecraft magnetometer measurements inherently include these deviations from the dipole field, they need to be represented in the simulated magnetometer or within the geomagnetic field models for accurate predictions of the near Earth magnetic fields.

In reality, neither the geomagnetic field models of the Earth nor the magnetometers are accurate. They both have various error sources resulting from several factors. The simulated

magnetometers include bias and noise errors. While in many studies, magnetic disturbances in space environment are treated as bias, in several others, they are accepted as noise [14,15]. However, in these studies, it should be remembered that the magnitude of the geomagnetic field deviations due to the magnetospheric storms can be obscured by the sensor-related noise used in the simulated magnetometers [16]. In order to estimate the magnetic moment of the satellite accurately, magnetometer bias resulting from other electrical devices on satellite should be estimated and removed precisely. Therefore, online and offline magnetometer calibration methods for time-variable errors arising from both magnetometer bias and the magnetic anomaly were introduced in [17] for two nanosatellites which need geomagnetic field data as accurate as possible for their mission requirements. In [17] and its extended version [18], the authors treated the magnetic anomaly as bias in the simulated magnetometer to improve the attitude estimation. In addition to the bias associated with the magnetic anomaly, they also added an additional magnetometer bias to build their simulated magnetometer. Both the magnetic anomaly bias and the magnetometer bias were used as the state vector elements within the simulated magnetometer. But, here we should also note that the magnetic anomalies in space environment are not the errors resulting from the magnetometer itself, but they are the magnetic deviations overlapped on the geomagnetic field resulting from the magnetic storms and magnetospheric substorms. In order words, they have a physical cause and their properties vary depending on the properties of the source and they cannot be predicted using linear models. Therefore, treating them as bias or noise error does not correctly take into account their true nature and their contribution in the measurements of simulated magnetometer. The studies in [17,18] treated the magnetic anomalies as a Gauss-Markov statistical process. Gauss-Markov model is a model frequently used to represent the sensor biases or disturbances [19–21]. However, it only depends on time and thus, it may be an inadequate representation of magnetic anomaly events which are linked to geomagnetic storm and magnetospheric substorms, since

these storms and substorms are not only time dependent but also their effects vary depending on the magnetic latitude, the height in the atmosphere, and the strength of the magnetospheric activity, i.e. magnetotail dynamics, but eventually on the solar activity [22–25]. While auroral substorms occur more frequently and affect high latitudes, variations in the ring current strength, or the motion of the magnetopause boundary affect the magnetic structure of the Earth at the equatorial latitudes [26 and references therein]. In addition, the magnetic anomalies associated with the magnetic storms increase during the high solar activity periods and decrease as the solar activity ceases. These indicate that it would be incorrect to consider them as noise. In [27], the authors stated that the magnetic anomalies should be modeled separately to avoid tuning problem but they stated that the external disturbances hard to model because of its complex ambient nature.

Early models of the Earth’s magnetic field represent only the dipole geomagnetic fields resulting from the Earth’s internal dynamo. The effects of magnetic disturbances are not included in these early models. As the satellite observations of the geospace environment increase, these models, consequently modelling the LEO environment, have been improved such that the physics of the magnetic environment were incorporated in the models. The IGRF model is one of these early models of the geomagnetic field used for attitude determination at LEO altitudes. The accuracy of the IGRF models was investigated in several studies and usually found satisfactory in predicting the satellite attitude [14,15,28].

First studies that take into account the effects of magnetic anomalies from the spacecraft attitude perspective are presented in [29–31]. These studies used IGRF and T89 models to evaluate the geomagnetic field at LEO altitudes during geomagnetically active days. T89 model developed by Tsyganenko in 1989 is an empirical geomagnetic field model [32,33] that was derived using large amount of magnetic field data of from 11 Earth-orbiting spacecraft measurements at various distances from LEO to 30 Earth Radii behind the Earth and thus

covering vast magnetospheric regions including plasmasphere, plasmashell, radiationbelts, neutral sheet, near Earth magnetospheric tail, and the magnetospheric boundary [34]. In contrast to IGRF model, the T89 model includes contributions from external magnetospheric sources such as ring current, magnetotail current system, magnetopause currents and large-scale system of field-aligned currents. The model employs several physical conditions such as dipole tilt angle effects, neutral sheet curvature and more or less realistic magnetopause boundary as well as the effects from the magnetospheric activity. In [29–31], the predicted and observed magnetic fields, and angles between magnetic field vectors from IGRF and T89 were analyzed for three selected geomagnetic storm events and compared the variations with those obtained during the quiet day. They showed that the T89 model gives closer magnetic field predictions to the observations, and the errors are smaller compared to those from the IGRF model. This further implies that the attitude angles will be estimated in a higher sensitivity if T89 model. It is of primary interest here to investigate the effects on geomagnetic disturbances on the satellite attitude angles (roll, pitch and yaw) using these models and quantify the effects. For this purpose, first we demonstrate how the angle between the magnetic field vectors predicted by the models varies with the increasing levels of geomagnetic activity. Then, we show that how these geomagnetic activity effects are propagated on to the satellite attitude angles.

Our second purpose in this paper is to explore the effect of the presence of one or more attitude sensors onboard the satellite in addition to the magnetometer. The sun sensors and gyroscopes are considered for this purpose. The mathematical models of these sensors can be implemented into the attitude estimation methods using e.g. Kalman-type filters. As the satellite's dynamical model and the simulated magnetometers are nonlinear, the extended Kalman filter (EKF) or its extensions can be used for obtaining the attitude angles [35]. Among the several types of the Kalman filters are Linear Kalman Filter (LKF), Extended Kalman Filter (EKF), Unscented Kalman Filter (UKF). In Kalman filters, generally all three of the attitude

sensors, namely sun sensor, magnetometer and gyroscope, are employed together to increase the accuracy in the attitude estimation [35–39]. However, the magnetometers can be used alone to estimate satellite's attitude in the absence of one or both of the other sensors. In this part, we utilize the various combinations of these sensors with EKF to compare the efficiency of the different sensor configurations under the low/high geomagnetic activity conditions. The configurations performed are magnetometer alone, magnetometer and gyroscope, magnetometer and sun sensor, and all sensor-configuration, i.e. magnetometer, sun sensor and gyroscope. While model predictions of the geomagnetic field are needed for all configurations, it is clear that it will be more important for the success of EKF procedure that uses magnetometer sensor configuration only.

The organization of the paper is as follows: Section 2 presents the satellite kinematic and dynamic equations while Section 3 describes the models, magnetic field and the sun direction vectors used for satellite attitude estimation, respectively. This is followed by the attitude estimation method based on traditional approach in Section 4. Section 5 shows how geomagnetic field models differ with the increasing level of geomagnetic activity. The analysis of the effects of the geomagnetic disturbances on the accuracy of the spacecraft attitude angles is presented in Section 6. Section 6 provides the results for four different sensors configurations. Finally, Section 7 concludes our study.

2. Satellite Equations of Motion

The orbit of the satellite is propagated in time using SGP4 model [40]. The satellite position data were used in ECEF (Earth Centered, Earth Fixed) using GEO (Geographic Coordinates). Angular motion of the satellite was defined in ECI (Earth Centered Inertial) system.

For the satellite rotational motion, equation of kinematics is represented in terms of Euler angles of yaw, pitch roll as,

$$\begin{bmatrix} \dot{\psi} \\ \dot{\theta} \\ \dot{\phi} \end{bmatrix} = \begin{bmatrix} 0 & \sin(\phi)/\cos(\theta) & \cos(\phi)/\cos(\theta) \\ 0 & \cos(\phi) & -\sin(\phi) \\ 1 & \sin(\phi)\tan(\theta) & \cos(\phi)\tan(\theta) \end{bmatrix} \begin{bmatrix} p \\ q \\ r \end{bmatrix}, \quad (1)$$

where p , q , r are the components of the ω_{BR} vector in body frame with respect to the reference (orbit) frame. The angular velocities (ω_{BI}) in the body axis can be expressed with respect to the inertial coordinate system as

$$\omega_{BI} = [\omega_x \quad \omega_y \quad \omega_z]^T, \quad (2)$$

and the angular velocities (ω_{BI} , ω_{BR}) have the relationship as,

$$\omega_{BR} = \omega_{BI} - \mathbf{A} [0 \quad -\omega_o \quad 0]^T, \quad (3)$$

where ω_o orbital angular velocity, computed as

$$\omega_o = (\mu / r_o^3)^{1/2}, \quad (4)$$

using μ -gravitational constant, r_o - distance between the satellite and Earth's centers. ω_o is constant for circular/near-circular orbits. \mathbf{A} represents the transformation matrix from orbit to body frame in terms of (3-2-1) Euler angles sequence [41] as,

$$\mathbf{A} = \begin{bmatrix} \cos(\theta)\cos(\psi) & \cos(\theta)\sin(\psi) & -\sin(\theta) \\ -\cos(\phi)\sin(\psi)+\sin(\phi)\sin(\theta)\cos(\psi) & \cos(\phi)\cos(\psi)+\sin(\phi)\sin(\theta)\sin(\psi) & \sin(\phi)\cos(\theta) \\ \sin(\phi)\sin(\psi)+\cos(\phi)\sin(\theta)\cos(\psi) & -\sin(\phi)\cos(\psi)+\cos(\phi)\sin(\theta)\sin(\psi) & \cos(\phi)\cos(\theta) \end{bmatrix}. \quad (5)$$

Dynamic equations are also obtained by the principle of conservation of angular momentum.

$$J_x \frac{d\omega_x}{dt} = N_x + (J_y - J_z)\omega_y\omega_z, \quad (6a)$$

$$J_y \frac{d\omega_y}{dt} = N_y + (J_z - J_x)\omega_z\omega_x, \quad (6b)$$

$$J_z \frac{d\omega_z}{dt} = N_z + (J_x - J_y)\omega_x\omega_y, \quad (6c)$$

where J_x , J_y and J_z inertial moment elements, N_x , N_y and N_z are the external disturbances affecting the satellite.

3. Components of Satellite Attitude Determination System

3.1. Geomagnetic Field Models

Among the several geomagnetic field models currently available in the literature, T89 and IGRF models were used to evaluate the attitude angles in this study. A brief introduction on the properties of these models are given below.

3.1.1. International Geomagnetic Reference Field Model

History of IGRF model goes back to 1900s. The model is revised every five years and released by the International Association of Geomagnetism and Aeronomy (IAGA). The 13th version of IGRF was released in 2020. IGRF only considers the internal dynamo currents that produce the Earth's magnetic field [5]. It is based on the dipole approximation of the Earth's magnetic field with the coefficients determined from the spacecraft magnetic field data using spherical expansion analysis with the coefficients determined from the spacecraft magnetic field measurements. The model includes series of the spherical harmonics at N=13th degree that are updated every 5 years. Equation (7) gives the expansion with the coefficients. The inputs (r, θ, ϕ, t) are the radial distance (km) from the centre of the Earth, co-latitude (deg), longitude (deg) of the satellite position at the specific time (t). In the equation, the global variables (g and h) are Gauss coefficients while P denotes the Legendre function.

$$\mathbf{B}_{INT}(r, \theta, \phi, t) = -\nabla \left\{ a \sum_{n=1}^N \sum_{m=0}^n \left(\frac{a}{r} \right)^{n+1} [g_n^m(t) \cos(m\phi) + h_n^m(t) \sin(m\phi)] \times P_n^m(\cos \theta) \right\}. \quad (7)$$

Here, \mathbf{B}_{INT} is the magnetic field in the units of nanoTesla (nT). The major axis of the Earth was accepted as 6378.137 km in the model. In this paper, the output magnetic field vector from the geomagnetic field model is shown as \mathbf{B}_{model} and it is given in magnetic (MAG) coordinates.

In MAG coordinate system, z-axis aligns with the dipole axis and y-axis is perpendicular to the plane containing the dipole axis and the rotation axis of the Earth. The x-axis completes the right-handed system. More information about the coordinate systems may be found in [42].

3.1.2. *Tsyganenko's Model*

The variations in space environment result from the solar and magnetospheric activity. The magnetosphere is highly dynamic especially during the strong solar disturbances. The currents from the geomagnetic tail during the geomagnetic storms and magnetospheric substorms produce variations in the geomagnetic fields at the LEO altitudes which are superimposed on the main geomagnetic field generated by the dynamo within the Earth's core. Consequently, it is expected that these external effects will affect the spacecraft attitude angles since they are determined by using the predictions of the geomagnetic field at the satellite altitudes. Therefore, it is anticipated that the inclusion of external effects in the predictions of geomagnetic fields will improve the accuracy of the attitude predictions. For this purpose, in this study, a second model, Tsyganenko 1989 model (T89) was used to predict the geomagnetic fields at the LEO orbit. Developed by Tsyganenko [32], T89 model is an empirical model based on large satellite data ranging from LEO altitudes to a distance of approximately 30 Earth radii. An analysis in the Van Allen belts is also possible when considering the satellites' altitudes used in the data sets [34]. The number of spacecraft data decreases with distance in the magnetosphere, but the available spacecraft data cover the most significant dynamic part of the magnetospheric regions on the dayside and night side, i.e. magnetotail. In the model, the total magnetic field was obtained by the sum of both internal (\mathbf{B}_{INT}) and external (\mathbf{B}_{EXT}) magnetic fields. Equation (8) gives the total magnetic field disturbance (\mathbf{B}_{EXT}) produced by the external sources only. While the main (internal) field (\mathbf{B}_{INT}) is obtained from IGRF as given in Equation (7), the magnetic field disturbance (\mathbf{B}_{EXT}) is obtained from T89. In this equation,

\mathbf{B}_{EXT} includes effects from magnetospheric ring current (\mathbf{B}_{ring}), tail current (\mathbf{B}_{tail}), magnetopause currents (\mathbf{B}_{mp}), and field aligned currents (\mathbf{B}_{FC}) (please see [32,43–47] for more details).

$$\mathbf{B}_{EXT} = \mathbf{B}_{ring} + \mathbf{B}_{tail} + \mathbf{B}_{mp} + \mathbf{B}_{FC}. \quad (8)$$

Since the external magnetic field (\mathbf{B}_{EXT}) is superimposed on the main geomagnetic field, T89 returns the total geomagnetic field as $\mathbf{B}_{model} = \mathbf{B}_{INT} + \mathbf{B}_{EXT}$ at the specified location. Therefore, T89 model is considered as an improved model over IGRF for predicting geomagnetic fields at LEO.

In T89 model, satellite data sets were categorized according to the geomagnetic activity index called K_p . K_p (planetary K-index) is an indicator of disturbances in the Earth's magnetic field and is used to characterize geomagnetic storms' magnitudes [48,49]. Thus, from the modelling point of view, it gives a measure of the strength of the external source. It is calculated globally using mid-latitude magnetic stations at every 3-hours and has a scale from 0 to 9 expressed in thirds of a unit with 28 values, e.g. 4- is 3 2/3, 4o is 4 and 4+ is 4 1/3 [50,51]. K_p greater than 4 indicates strong geomagnetic activity in the magnetosphere. IOPT indicates the number used in the T89 algorithm related to activity level. Even though the level of activity can rise up to $K_p = 9$, the highest K_p accepted within T89 code is 6- because of the smaller number of satellite data for higher K_p levels larger than 6-.

Table 1. K_p index and model parameter IOPT range in T89 model.

IOPT	1	2	3	4	5	6	7
K_p	0o, 0+	1-, 1o, 1+	2-, 2o, 2+	3-, 3o, 3+	4-, 4o, 4+	5-, 5o, 5+	>=6-

3.2. Simulated Magnetometer Measurements

Because the magnetometers are cheap, reliable and light weight, they are the most widely used sensors for the determination of the attitude angles on LEO satellites. Satellite's angular motion is determined by defining the dynamics and kinematics of the satellite. Then, the Euler angles are found for each magnetic field model representation. The magnetometer measurements of the real space environment can be simulated as:

$$\mathbf{B}_m(k) = \mathbf{A}(k)\mathbf{B}_o(k) + \mathbf{v}_B(k), \quad (9)$$

where $\mathbf{B}_o(k)$ is the geomagnetic field vector components in the orbital frame that were found using a geomagnetic field model, $\mathbf{B}_m(k)$ represents the simulated magnetometer measurements in the body frame, $\mathbf{v}_B(k)$ is the zero-mean Gaussian magnetometer measurement noise, and $\mathbf{A}(k)$, is the transformation matrix from orbit to body frame. In this equation, $\mathbf{B}_o(k)$ is obtained using:

$$\mathbf{B}_o(k) = \mathbf{L}(k)\mathbf{B}_{\text{model}}(k), \quad (10)$$

where $\mathbf{B}_{\text{model}}$ is the geomagnetic field vector obtained from a geomagnetic model, such as IGRF or T89 in our case, and $\mathbf{L}(k)$ indicates the transformation matrix from MAG coordinates (see Section 3.1.1) to orbital coordinate system. The success of the simulated magnetometer depends on how accurately these terms are predicted.

3.3. Simulated Sun Sensor Measurements

Another attitude sensor used to predict the satellite's attitude is the sun sensor which determines the sun direction vector whenever sun is visible. The sun direction model can be found in [52]. The sun direction vector measurements can be expressed in the following form:

$$\mathbf{S}_m(k) = \mathbf{A}(k)\mathbf{S}_o(k) + \mathbf{v}_S(k), \quad (11)$$

where $\mathbf{S}_m(k)$ is the measured sun direction vector as the direction cosines in body frame, $\mathbf{S}_0(k)$ represent the sun direction vector in the orbit frame as a function of time and orbit parameters, and $\mathbf{v}_s(k)$ is the zero-mean Gaussian sun sensor measurement noise.

3.4. Simulated Rate Gyro Measurements

Rate gyros are used in order to measure the angular velocity of the satellite. The measurements can be modeled as,

$$\boldsymbol{\omega}_m(k) = \boldsymbol{\omega}_{BI}(k) + \mathbf{v}_g(k), \quad (12)$$

where $\boldsymbol{\omega}_m(k)$ is the measured angular rates of the satellite body frame with respect to the inertial frame, and $\mathbf{v}_g(k)$ is the zero-mean Gaussian gyroscope measurement noise.

4. Attitude Estimation Algorithm

For the satellite attitude and rate estimation, 6-dimensional state vector $\mathbf{x}(k+1)$ is composed of attitude angles (ψ yaw; θ pitch; ϕ roll) and angular rates (ω_x angular velocity in x axis, ω_y angular velocity in y axis, ω_z angular velocity in z axis). All three attitude angles describe the deviation between the orbit and the body reference frame.

$$\mathbf{x}(k+1) = [\psi(k+1) \ \theta(k+1) \ \phi(k+1) \ \omega_x(k+1) \ \omega_y(k+1) \ \omega_z(k+1)]^T. \quad (13)$$

The satellite's rotational motion can be represented using nonlinear mathematical model about its mass center driven by Gaussian white noise with white noise-corrupted measurements defined by,

$$\mathbf{x}(k+1) = \mathbf{f}[\mathbf{x}(k), k] + \mathbf{w}(k), \quad (14)$$

$$\mathbf{z}(k) = \mathbf{h}[\mathbf{x}(k), k] + \mathbf{v}(k), \quad (15)$$

where $\mathbf{z}(k)$ is the measurement vector at time k , $\mathbf{w}(k)$ is the system noise, $\mathbf{v}(k)$ is the measurement noise, $\mathbf{f}[\mathbf{x}(k), k]$ is the nonlinear state transition function mapping the previous state to the current state, $\mathbf{h}[\mathbf{x}(k), k]$ is a nonlinear measurement model mapping current state to measurements. It is assumed that both noise vectors $\mathbf{v}(k)$ and $\mathbf{w}(k)$ are linearly additive Gaussian, temporally uncorrelated with zero mean with the corresponding covariance matrices \mathbf{Q} and \mathbf{R} respectively. It is assumed that process and measurement noises are uncorrelated.

We consider a real-time linear Taylor approximation of the system function at the previous state estimate and that of the observation function at the corresponding predicted position. The Extended Kalman Filter (EKF) algorithm is used for this purpose [53,54]. The EKF is applied using different sensor configurations on LEO satellite in order to evaluate the magnetic anomaly effects on the attitude estimation system (see Appendix for the details of filter design). The scheme of the traditional EKF used in this paper is presented in Fig. 1. Magnetometer is the base sensor as it is used in all of the sensor configurations considered in this paper. Four different sensor configuration scenarios are implemented within the algorithm: 1. magnetometer only, 2. magnetometer and gyroscope, 3. magnetometer and sun sensor, 4. all sensors (magnetometer, sun sensor, and gyroscope). In the traditional approach (see Fig. 1), measurement models are based on nonlinear models of reference directions. Therefore, there is a nonlinear relation between the measurements and the states.

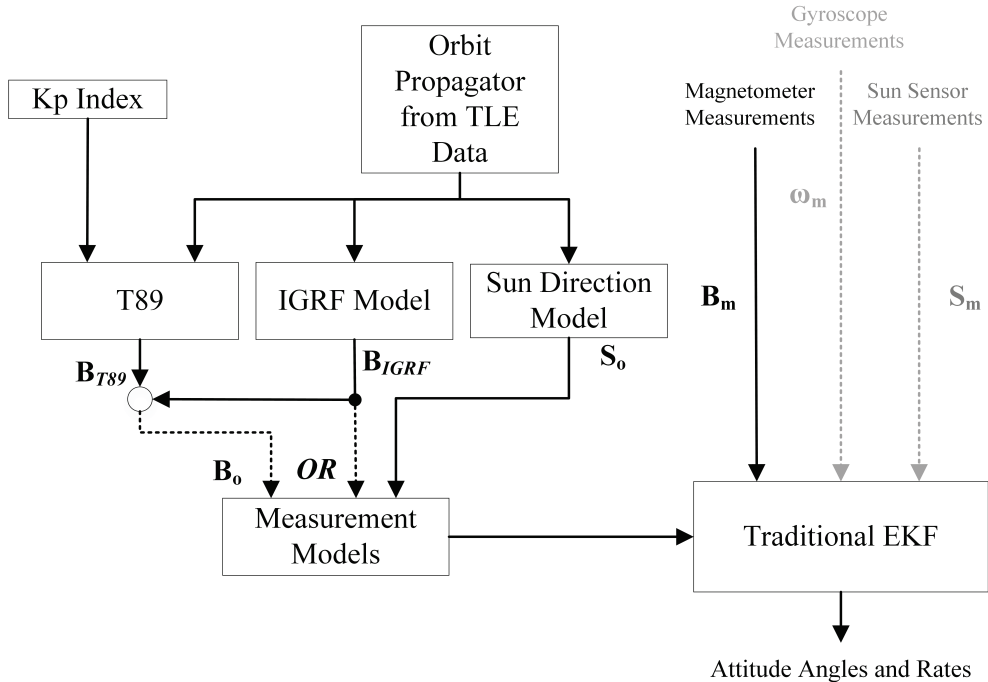


Fig. 1. Attitude estimation scheme using different magnetic field models and different sensors. \mathbf{B}_{T89} and \mathbf{B}_{IGRF} represent magnetic field models, T89 and IGRF, respectively. \mathbf{B}_o and \mathbf{S}_o are

the outputs from the geomagnetic field model and Sun direction model, both in the orbital frame. Also \mathbf{B}_m , \mathbf{S}_m , and ω_m are the magnetometer, sun sensor and gyroscope measurements in body frame. IGRF uses the position of the satellite, and orbital parameters to find the magnetic field vector in orbital frame. Inputs for the T89 model are the K_p index, position of the satellite and outputs from IGRF model for background geomagnetic field. In this algorithm, after the orbit propagation from TLE data, position of the satellite for selected time interval and sampling time were obtained in spherical coordinates and transformed into Cartesian (ECEF).

The four scenarios that use magnetic field predictions from both T89 and IGRF were adopted in the traditional EKF in the order given above. As magnetometers, the sun sensors are the other instruments used very commonly in satellite missions, therefore, it would be interesting to see how its presence affects the accuracy of satellite attitude.

5. Dependence on Geomagnetic Activity

Magnetic field measurements from magnetometers on board two different satellites at LEO orbit were analyzed and compared with those from IGRF and T89 models in [29] for three cases of selected geomagnetic activity events. The study in [29] demonstrated that both models indicate differences with the on-board magnetic fields regardless of the activity level, but more so when the activity level is high. Further, it was also shown that IGRF model gives larger differences compared to T89 model during both quiet and active times, with larger differences with increasing activity. During geomagnetically active day, T89 model gave closer estimations to the on-board observations. While the main purpose of current paper is to investigate the effects of magnetospheric activity on the satellite attitude angles estimated by EKF, we first demonstrate the dependence of the angle between the predicted magnetic fields of the models on the increasing levels of geomagnetic activity. This is accomplished by using the increasing levels of activity K_p in T89 model and calculating the angle between the predicted magnetic field from both T89 and IGRF models. IGRF is a function of time and position but independent of activity; however, it is used here as background geomagnetic levels to detect the deviations resulting from the geomagnetic activity. The calculated angle is, then, used as input in EKF analysis to calculate the attitude angles (yaw, pitch and roll) and for four different sensor configurations.

Before demonstrating the effects of the geomagnetic activity, we present Figure 2 in order to give an idea on the order of the disturbance fields, i.e. \mathbf{B}_{EXT} , seen in panel e. From top to bottom, Figure 2 shows K_p (panel a), noise (panel b), constant bias (panel c), accumulated bias (panel d), and disturbance field (panel e) along the satellite trajectory. In order to create this figure, we run T89 model for the selected K_p variation seen in panel a. Since the simulated magnetometer uses the components seen in panels b, c, d, and e to simulate the geomagnetic

field anomaly, it is of purpose here to illustrate how independent of these components from geomagnetic activity level and how the disturbance field vary for the selected geomagnetic activity level given in panel a. Figure 2 indicates that naturally, the noise, constant bias, and accumulated bias are seen to vary independent of the geomagnetic activity level by their description, while disturbance field in panel e indicates variations from 0 to -8 nT for $K_p = 5$ and from 0 to ± 15 nT for $K_p = 6$ in panel a and increasing with the increased levels of K_p .

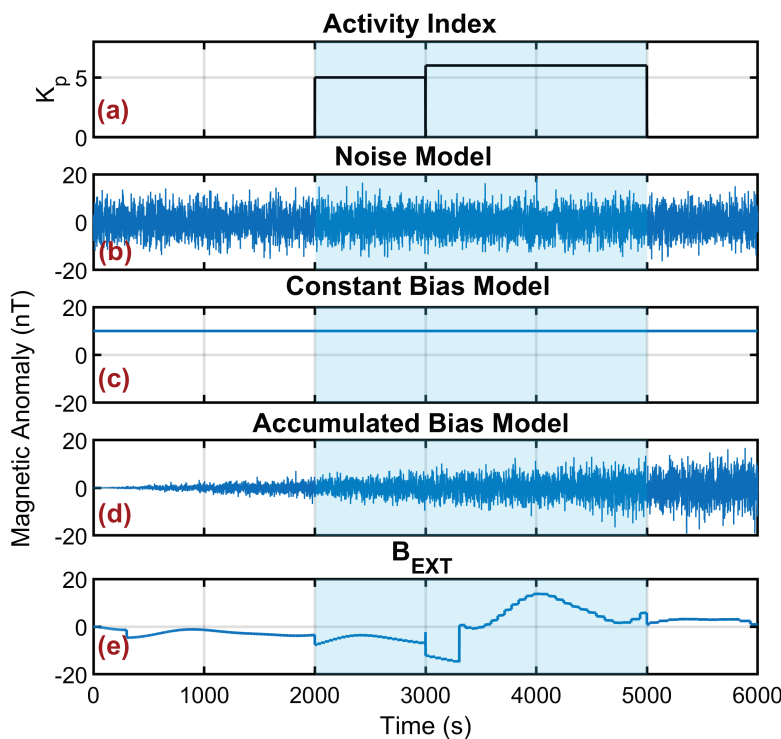


Fig. 2. Noise, constant bias, accumulated bias, and a sample of external magnetic field disturbance for different K_p levels.

Next, we demonstrate how the angle between the magnetic fields estimated from IGRF and T89 models. For this purpose, we consider a hypothetical nanosatellite with principal moments of inertia $J = \text{diag} [2.1 \times 10^{-3} \quad 2.0 \times 10^{-3} \quad 1.9 \times 10^{-3}] \text{ kg m}^2$. The orbit is almost circular with inclination $i = 87.4^\circ$, eccentricity $e = 0.0009$, average altitude 600 km, and orbital period of approximately 6000 seconds. The satellite is tumbling with the initial state of

$\mathbf{x}_0 = [0.03 \text{ rad} \quad 0.02 \text{ rad} \quad 0.01 \text{ rad} \quad 0.001 \text{ rad/s} \quad 0.0015 \text{ rad/s} \quad 0.002 \text{ rad/s}]^T$ as described in Equation (13). For this designed orbit, T89 model run for each K_p levels varying from 0 to 6. Since IGRF does not have a dependence on K_p , it was run only once. In Fig. 3, the angle between the predicted magnetic fields of T89 and IGRF was plotted in a box-plot as a function of the activity level (IOPT) given in the horizontal axis. In the figure, the box gives the quartile range from 25% to 75% with a dent indicating the median. The dotted lines above and below each box identify the range of potential outliers where the maximum and minimum for each box lie. While the red solid line gives a line fit to the average in each box, the box colors only identify the different K_p levels. Figure clearly shows that with the increasing levels of geomagnetic activity, the angle between the model predictions increases. Moreover, increased range of the outliers from the upper edge of the box indicates the increased scatter in the angle with the increased activity level. The differences in the angle can come from the activity level but also from the latitudinal variation of the moving spacecraft. Since both IGRF model and T89 model includes the same latitudinal variations in their background geomagnetic field predictions, we attribute the variations seen in this figure to the geomagnetic variations resulting from the storms and substorms in the magnetosphere at the satellite location, which otherwise expect the angle to be zero. While both average and median angles show increase with the increasing activity level, the maximum difference is found to be 18° corresponding to the highest level of activity in T89 model. These results confirm the case studies presented in [29] in a statistical sense based on model simulations.

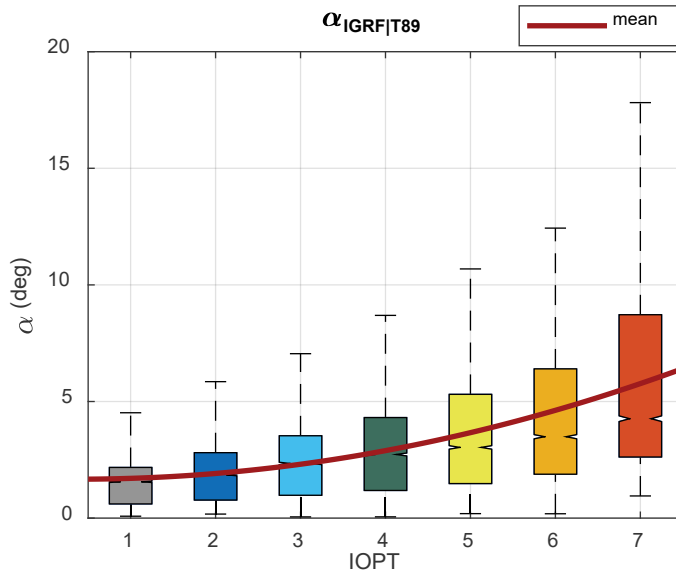


Fig. 3. Angle between IGRF and T89 magnetic field vectors for different K_p levels in T89 model.

Next, to isolate the effects of the geomagnetic activity on the angle with respect to the satellite position, i.e. the latitude of the satellite, we split Figure 3 into three categories according to the latitude (λ) of the spacecraft as low latitudes ($0^\circ \leq \lambda < 30^\circ$), mid-latitudes ($30^\circ \leq \lambda < 50^\circ$) and high latitudes ($\lambda \geq 50^\circ$). The result is given in Figure 4 where panels a, b, c are for low, mid- and high latitudes. As in Figure 3, horizontal axis represents the activity level (K_p). Figure 4 illustrates that as the activity increases, the angle increases gently at all latitudes which means geomagnetic activity affects the angle at all latitudes at some degree being maximum for $K_p > 6$ at 6° for low latitudes, 5.5° for mid-latitudes, and 12° for high latitudes. It is interesting to note that when $K_p = \{0o, 0+\}$, namely, when there is almost no geomagnetic activity, the results indicate a difference between the IGRF and T89 model field predictions at about 2° at all latitudes. This may be due to the fact that there are 30 coefficients defined for each IOPT level in T89 model. IOPT = 1 in T89 model, corresponds to $K_p = \{0o, 0+\}$ (see Table 1) and thus to non-zero coefficients which in turn give non-zero angles. The highest difference, on the

other hand, is seen at high latitudes at 12°. Moreover, panel c shows that the highest scatter, indicated by the level of the outliers, is seen at high latitudes as the level of activity increases. It is the smallest at low latitudes. This suggests that the high latitudes are more prone to the errors in the geomagnetic field orientations and thus in the angles.

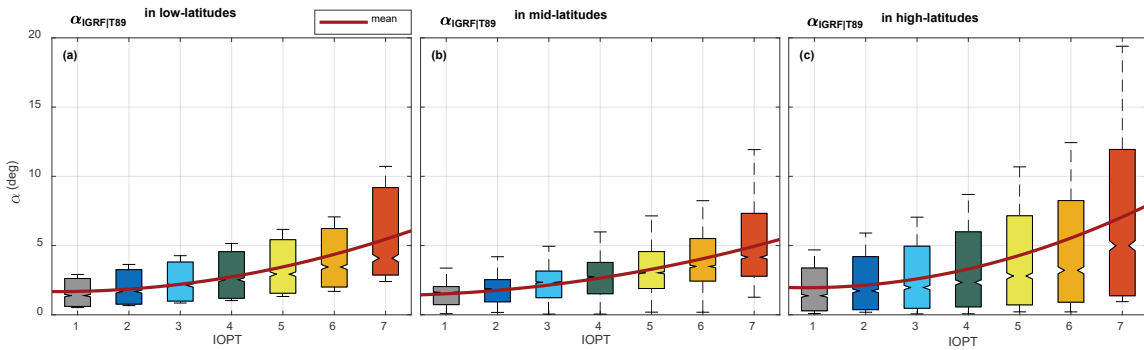


Figure 4. Variations in angle with geomagnetic activity for low- (a), mid- (b) and high- (c) latitudes.

Another way of showing the differences between two models involves the height variations of the geomagnetic field anomaly effects predicted by the models. This is demonstrated in Figure 5. Figure 5 illustrates the ratio between predicted external component (\mathbf{B}_{EXT}) to the total magnetic field ($\mathbf{B}_{model} = \mathbf{B}_{INT} + \mathbf{B}_{EXT}$) obtained from T89 model for $IOPT=1$ and $IOPT=7$ that correspond to quiet and active times with respect to various altitudes starting from 500 km to 20000 km. For this purpose, T89 model run for each $IOPT$ levels at each altitude along the orbit. At the end, the orbital average at each altitude was plotted. Figure shows that the magnetic field anomalies affect the satellite more at higher altitudes as expected. At the beginning, for the altitude of 500 km, the mean rate is around 3% and 11% for $IOPT=\{1, 7\}$ respectively. For the altitude of 20,000 km, the mean rate is around 10% and 42% for $IOPT=\{1, 7\}$ respectively. The average effect of the external field over different altitudes presented in Fig. 5 is found as 6% with $\bar{\mathbf{B}}_{EXT} = 24.6$ nT for $IOPT = 1$ and 23% $\bar{\mathbf{B}}_{EXT} = 109.3$ nT for $IOPT = 7$.

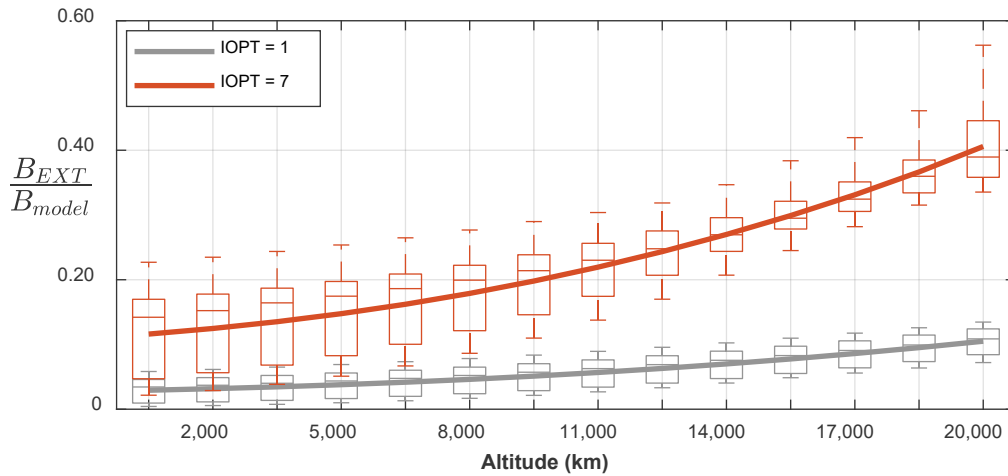


Figure 5. Dependence of external field (B_{EXT}/B_{model}) on satellite's altitude obtained from T89 model for IOPT = 1 and IOPT = 7 in T89 model.

6. Influence of the Geomagnetic Activity on the Accuracy of Attitude

Previous section showed that geomagnetic activity increases the angles between the predicted magnetic fields by the models and the differences in angles at different K_p levels are largest at high latitudes. It is thus expected that these differences in the angles will propagate to the attitude angles which is the main subject in this section. The actual attitude angles of roll, pitch, and yaw are calculated using satellite's orbital motion and the estimated ones using EKF procedures were compared for the quiet (IOPT = 1 for T89) and active (IOPT = 7 for T89) geomagnetic days. The magnetic field vectors needed to estimate the attitude angles were obtained from the T89 and IGRF models and simulated satellite measurements. The satellite specifications used in this section is provided in the previous part. Additionally, the sun sensors and magnetometers have 3-axis measurements and both sensors have 1-Hz frequency; estimation time step is also 1 sec. The sensor noises are characterized using normalized standard deviations $\sigma_B = 0.008$ for magnetometers, $\sigma_S = 0.002$ for sun sensors and the standard deviation of $\sigma_g = 0.005$ rad/s for rate gyros. We consider attitude estimation over a

single orbit (6000 s). Satellite's angular motion is determined by defining the dynamics and kinematics of the satellite which is described in Section II. In the following sections, extended Kalman filter is used in its traditional form, and the simulation results are presented for four different sensor configurations mentioned in Section IV as scenarios.

Fig. 6 presents the attitude angles estimated by EKF approach using the geomagnetic fields obtained from T89 model for the selected LEO satellite for active geomagnetic conditions and for magnetometer only scenario (i.e. scenario 1). In the figure, solid line gives the estimated attitude angles while dotted line presents the actual attitude angles obtained from Eq. (1). The panels from top to bottom are roll, pitch, and yaw. The horizontal axis on the panels is the time in seconds.

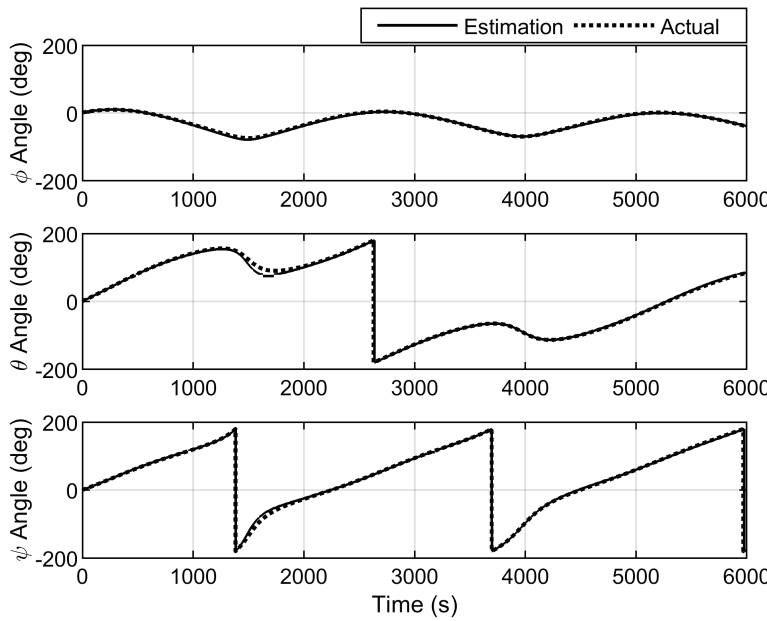


Fig. 6. Estimated and actual attitude angles using T89 model in traditional EKF for the active geomagnetic conditions and for magnetometer configuration only (scenario 1).

Fig. 6 shows that the differences between the estimated and actual attitude angles are noticeable but very small to be distinguished by eye. Actual attitude angles are computed using Eq. (1). We carried out the same analysis for all sensor configurations. The results were found to be very similar. We find that the differences between estimated and actual attitude angles are not large. Though small, it is of interest to quantify the difference. We carry out an error analysis

for this purpose. For error analysis, we use two methods: One is the mean of the differences between the estimated and actual attitude angles, namely $\frac{1}{N} \sum_{k=1}^N \mathbf{e}_k$ in degrees, where $\mathbf{e}_k = \hat{\mathbf{x}}(k+1) - \mathbf{x}(k+1)$ and the other is the Normalized Root Mean Square Error (NRMSE) calculated as $\left(\frac{100}{\bar{\mathbf{x}}} \sqrt{\frac{1}{N} \sum_{k=1}^N (\mathbf{e}_k)^2} \right)$ in percentages. Here $\hat{\mathbf{x}}(k+1)$ represents the estimated attitude angles using EKF, $\mathbf{x}(k+1)$ is the actual attitude angles, $\bar{\mathbf{x}}$ is the average of the actual attitude angles, and N is the number of data during the simulation we studied. The error (RMSE) is evaluated in Figures 7a and 7b, NRMSE results are discussed in Table 2.

We use IGRF results to represent the undisturbed conditions since IGRF model is independent of the geomagnetic activity. Figure 7a shows how each attitude angle component estimated by EKF using IGRF varies corresponding to each scenario. Different colors in this panel correspond to different scenarios. The panel shows how the errors corresponding to different scenarios are distributed for each attitude angle. Fig. 7b, on the other hand, presents how the errors corresponding to attitude angles are distributed for each scenario. Different colors in this panel correspond to different attitude angles such as black for roll, blue for pitch and pink for yaw angles.

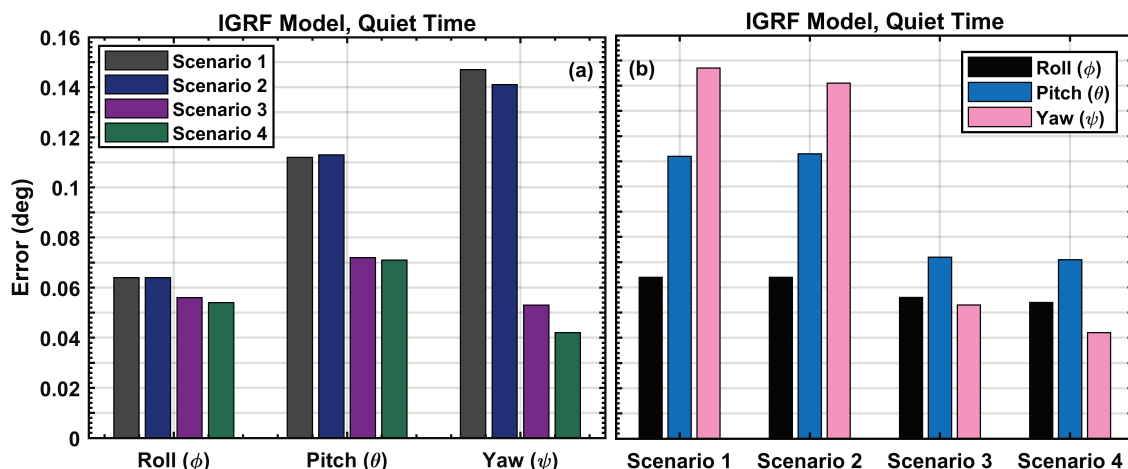


Fig. 7. Estimated errors using IGRF model during quiet time for each attitude component (a) and for each scenarios (b).

Representing quiet conditions, both figures give the following results:

1. The errors corresponding to all directional angles (roll, pitch and yaw) are larger in the order of scenario 1, scenario 2, scenario 3 and scenario 4, respectively. Magnetometer only scenario gives the largest error while the smallest error is obtained when all sensors (scenario 4) were used in attitude estimation. This result indicates that some of the errors caused by the IGRF estimation of geomagnetic fields are compensated by the addition of other two sensors. In other words, adding sun sensor and gyroscope reduces attitude estimation error. However, comparing the errors for scenario 2 and scenario 3, it can be clearly noticed that the presence of sun sensor reduces the error more compared to the error reduction by gyroscope.
2. It is clearly seen that the errors corresponding to pitch and yaw angles are the largest for scenario 1 and scenario 2 compared to those for roll angle, since the roll angle takes smaller values than the other two in the tumbling for our case (see Fig. 6). Here, the error levels may differ if the initial conditions are changed. All sensor scenario or magnetometer and sun sensor scenarios gives the better estimates for pitch and yaw angles compared to those of magnetometer only or magnetometer and gyroscope scenarios.
3. The errors corresponding to roll angle are at the same order for all scenarios and differences between the scenarios are negligible. The roll angle seems to be insensitive to which sensor is used on the satellite. Even though scenario 4 is slightly better, only magnetometer scenario gives as good estimate as all sensor scenario. Adding sun sensor and gyroscope does not make an appreciable difference in reducing the errors in the yaw angle.

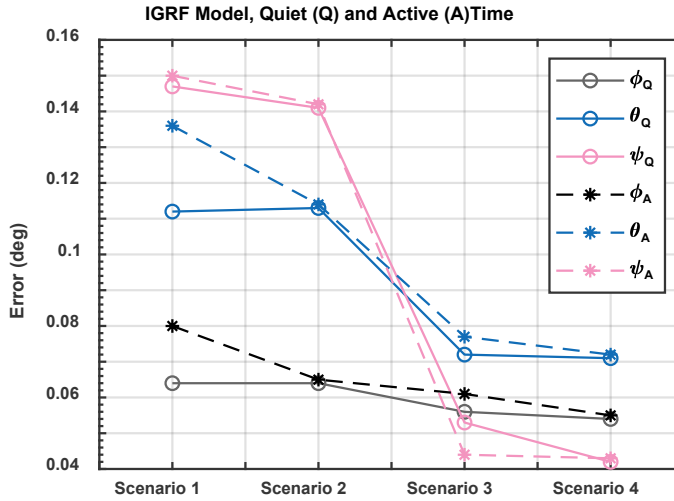


Figure 8. Estimated errors for IGRF model predictions of the attitude angles during the quiet (solid) and active (dashed) geomagnetic conditions.

Similar evaluations for IGRF model during active conditions can also be derived. Figure 8 is performed for this purpose and illustrates the errors obtained during quiet (solid lines) and active (dashed lines) times. The figure also compares the quiet and active day performance of the IGRF model between different scenarios. It is clear that the scenario 1 and 2 give higher errors for the active times for all attitude angles. The highest difference between active and quiet time errors is seen in scenario 1 while other scenarios do not seem to be affected by the geomagnetic disturbance much and present smaller difference.

Figs. 9a and 9b are generated to demonstrate the differences calculated by subtracting T89 errors from those of IGRF for quiet (panel a) and active days (panel b) respectively. Positive differences indicate that IGRF errors are larger than those of T89. In both panels, it is clear that the errors associated with IGRF model are larger than those of T89 for all attitude angles. Also, both panels show that the largest differences between the models for both activity levels occur in pitch and yaw angles in case of scenario 1 and scenario 2. It can also be seen that the error differences are larger for active days especially for scenario 1 indicating the effect of the geomagnetic disturbances on the magnetometer measurements.

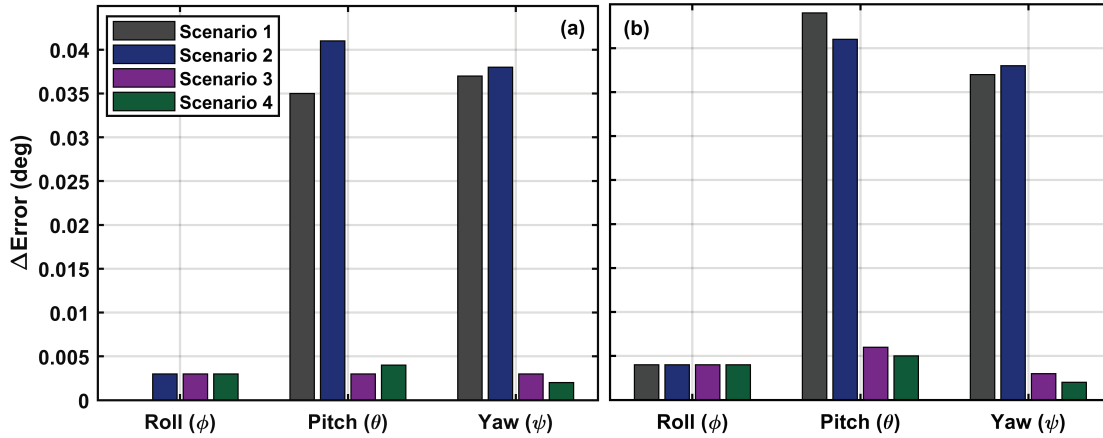


Fig. 9. Differences between the errors associated with both models for quiet (a) and active (b) days.

Lastly, we present Table 2 that displays the results of NRMSE to illustrate how the errors depend on the sensor configurations for both quiet (blue highlight) and active (yellow highlight) geomagnetic conditions. In the table, ϕ , θ , and ψ represent the roll, pitch and yaw angles respectively. Since the geomagnetic disturbance effects are found to be larger in case of scenario 1 for especially pitch angle, the results in Table 2 are evaluated by comparing IGRF and T89 model performances for scenario 1 only and the addition of other sensors are evaluated qualitatively as same as given above. For scenario 1, we see that using the T89 model reduces the error and improves the attitude angles (roll, pitch and yaw) by 0.03%, 0.06% and 0.01% respectively during the quiet times and 0.02%, 0.02%, and 0.02% during the active geomagnetic conditions.

Table 2. NRMSE between estimated and actual attitude angles.

Geomagnetic State	NRMSE (%)	Scenario 1		Scenario 2		Scenario 3		Scenario 4	
		Mag. only		Mag. and Gyroscope		Mag. and Sun sensor		All sensors	
		IGRF	T89	IGRF	T89	IGRF	T89	IGRF	T89
Quiet	ϕ	0.72	0.69	0.67	0.66	0.03	0.03	0.02	0.02
	θ	0.50	0.44	0.36	0.34	0.03	0.02	0.01	0.01
	ψ	3.18	3.17	3.17	3.16	0.25	0.23	0.22	0.21
Active	ϕ	0.77	0.75	0.68	0.66	0.04	0.03	0.02	0.02
	θ	0.52	0.50	0.37	0.34	0.06	0.04	0.03	0.02
	ψ	3.20	3.18	3.17	3.17	0.27	0.25	0.24	0.23

As a summary, Table 2 indicate that the magnitude of errors in all angles is small for both quiet and active conditions which indicates that the attitude estimations are not severely affected by the geomagnetic disturbances. We can say that using T89 as the geomagnetic model improves the attitude predictions at least 0.01 % over using IGRF depending on the sensor configurations and reduces the errors in all attitude angles. Especially during the active days, this improvement is noticeably clear. As a result of these comparisons, whether IGRF model or T89 model should be used when calculating the attitude angles at LEO altitudes depends on the intended accuracy of the attitude angles determined by the mission requirements. If the computational load on on-board computers of the satellite is considered, then one may use conventional model IGRF as the geomagnetic field model of the satellite attitude since its model inputs are simpler. We showed that although small, the errors and the performance of attitude estimation methods depend on which geomagnetic field model used, i.e. whether it is IGRF or T89 in this case. We suggest that the most recent modelling techniques, such as T89, will be still an advantage when determining the attitude angles even during the undisturbed conditions, but more so under disturbed conditions.

Overall evaluation for IGRF indicates that the model produces larger errors in attitude angles during active days with respect to the quiet days for all four sensor configurations. On the second hand, adding other sensors seem to improve the errors resulting from the disturbances superimposed on the quiet time background geomagnetic field.

In this study, we have also calculated the performance of the models with different sensor configurations as scenario 1, scenario 2, scenario 3, and scenario 4. Adding gyroscope to magnetometer to improve the attitude angles does not make a considerable reduction in the errors during quiet times in all attitude angles. However, adding sun sensor improves the errors at these times. Table 2 indicates that gyroscope reduces the errors by about 0.07% on the average for all attitude angles with respect to scenario 1. Also, it reduces the errors by 0.02%

in scenario 4 with respect to scenario 3. The sun sensor in scenario 3, on the other hand, reduces the errors by about 1.4% on the average with respect to the scenario 1; and by 1.3% in scenario 4 with respect to scenario 2. All sensors scenario has the smallest errors for the quiet days. However, the decrease in error is not due to the presence of gyroscope but presence of sun sensor in this scenario. Use of gyroscope sensor in spacecraft attitude becomes more important in the absence or failure of the sun sensors. Earth's shadow or the eclipse period creates such unfavorable space conditions. To prevent the satellite from the effects of the eclipse, it is very common to use both magnetometers and gyroscope together for attitude purposes. Here, we showed that the gyroscopes do not provide a better estimate of attitude angles during the quiet times against using magnetometers only. However, using gyroscope during the active times together with magnetometers reduces the errors in the prediction of attitude angles. On the contrary to gyroscopes, use of sun sensors makes large improvement in reducing the errors in the estimated attitude angles during both quiet and active times. Between IGRF and T89 models, our comparisons show that using T89 model in all scenarios, slightly but still, improves the estimated attitude angles. The only disadvantage that this will bring may be the increase in the computational load on the on-board computers.

7. Conclusions

In this paper, the geomagnetic field models that are used to estimate the geomagnetic fields and satellite attitude angles were studied during the geomagnetically active and quiet days. It is the first time that the attitude angles (yaw, pitch, and roll) were studied using a global empirical model, T89 model, of the magnetosphere which takes into account the magnetic disturbances resulting from the magnetospheric substorms and/or geomagnetic storms and compared with the results from the more conventional model, IGRF. Our analysis showed that the angles between the geomagnetic field vectors estimated by the models increases as the

geomagnetic activity increases from quiet levels ($K_p = 0$) to strongly active days ($K_p \geq 6$) and it increases more over the high latitudes than over the equatorial regions especially during the strong activity days for $K_p \geq 6$. Similarly, it was shown that the magnetic field disturbances estimated from T89 at LEO are higher during the high geomagnetic activity as the satellite altitude becomes higher. Since this angle is one of the inputs in the estimation of the satellite attitude angle by EKF, the satellite attitude angles will be sensitive to its variations. Thus, it is expected that the attitude angles will increase as the geomagnetic activity enhances, especially at the high latitudes and at high altitudes.

Secondly, we have shown that although small, differences occur between the estimated attitude angles using T89 and IGRF models during the active days. When we have analyzed magnetometer only case, we found that the errors in the predicted attitude angles using IGRF model are larger than the errors obtained by suing T89 model. We also showed that T89 model estimates smaller errors in the EKF estimated attitude angles during the active days. The largest errors were obtained for pitch and yaw angles during both quiet and active days.

Additionally, we used traditional EKF to estimate the attitude angles for different sensor configurations including magnetometer, sun sensor, and gyroscope for quiet and active times. We studied if the addition of other attitude sensors on board will change the accuracy of the estimated attitude angles during both quiet day and active days. We showed that the highest errors in the estimated attitude angles were obtained for magnetometer only and magnetometer plus gyroscope scenarios during the quiet days. Also, we found that during the quiet days, while presence of sun sensor reduces the errors in the estimated attitude angles, gyroscope has less effect in the reduction of the errors. During the active days while all scenarios give small errors, the magnetometer only and magnetometer and gyroscope scenarios show markedly highest errors. The errors resulting from the geomagnetic disturbances are reduced drastically

after we added the sun sensor measurements into the system. The most accurate results with the smallest errors were obtained for all sensor scenario. In this case, the predicted attitude angles were significantly improved and obtained close to the actual attitude angles. This study emphasizes on the importance of the effects that the magnetic disturbances will have on the attitude angles and helps to choose the right sensor combination during both quiet and disturbed times for a better attitude estimation.

Acknowledgment

D. Cilden-Guler is supported by ASELSAN and TUBITAK PhD scholarships. We communicated with Dr. Nikolai Tsyganenko at Saint-Petersburg State University for the most updated version (T89d) of the Tsyganenko models.

Appendix. Extended Kalman Filter for Satellite's Attitude Estimation: Traditional Approach

The traditional approach to satellite's attitude estimation is to use an extended Kalman filter (EKF) [35,55]. The traditional EKF design is given in this section for estimating the states in Equation (13). The prediction of the filter can be expressed as,

$$\hat{\mathbf{x}}(k / k-1) = \mathbf{f}[\hat{\mathbf{x}}(k-1), k-1] \quad (\text{A.1})$$

using the state transition (system) function defined in Equations (1) and (6) respectively for the kinematics and dynamics equations of the satellite's rotational motion.

The state estimation can be found as,

$$\hat{\mathbf{x}}(k) = \hat{\mathbf{x}}(k / k-1) + \mathbf{K}(k) \{ \mathbf{z}(k) - \mathbf{h}[\hat{\mathbf{x}}(k / k-1), k] \} \quad (\text{A.2})$$

The filter-gain of EKF is,

$$\mathbf{K}(k) = \mathbf{P}(k / k-1) \mathbf{H}^T(k) \left[\mathbf{H}(k) \mathbf{P}(k / k-1) \mathbf{H}^T(k) + \mathbf{R} \right]^{-1} \quad (\text{A.3})$$

where $\mathbf{H}(k) = \frac{\partial \mathbf{h}[\hat{\mathbf{x}}(k/k-1), k]}{\partial \hat{\mathbf{x}}(k/k-1)}$ is the measurement matrix consisting of partial derivatives of measurement function with respect to the states. The measurement models for $\mathbf{h}[\cdot]$ are given in Equations (9), (11), (12) for magnetometer, sun sensor and gyroscopes respectively. The covariance matrix of the prediction error is,

$$\mathbf{P}(k/k-1) = \frac{\partial \mathbf{f}[\hat{\mathbf{x}}(k-1), k-1]}{\partial \hat{\mathbf{x}}(k-1)} \mathbf{P}(k-1/k-1) \times \frac{\partial \mathbf{f}^T[\hat{\mathbf{x}}(k-1), k-1]}{\partial \hat{\mathbf{x}}(k-1)} + \mathbf{Q} \quad (\text{A.4})$$

The covariance matrix of the filtering error is,

$$\mathbf{P}(k/k) = [\mathbf{I} - \mathbf{K}(k)\mathbf{H}(k)]\mathbf{P}(k/k-1) \quad (\text{A.5})$$

The filter expressed by Equations (A.1) - (A.5) is called the EKF based on traditional approach. In this study, four different sensor configuration scenarios are implemented within the algorithm: 1. magnetometer only, 2. magnetometer and gyroscope, 3. magnetometer and sun sensor, 4. all sensors (magnetometer, sun sensor, and gyroscope). Therefore, the measurement vector (\mathbf{z}) is composed of different sensor measurements in every scenarios (see Table A.1). The filter design does not change except the related matrices (\mathbf{H} , \mathbf{R}) calculated based on the measurement vector. Their dimensions are given in Table A.1 as well.

Table A.1. EKF parameters for different scenarios.

Scenario	Measurement vector	\mathbf{H} matrix dimension	\mathbf{R} matrix dimension
1	$\mathbf{z} = \mathbf{B}_m$	3x6	3x3
2	$\mathbf{z} = [\mathbf{B}_m \quad \boldsymbol{\omega}_m]^T$	6x6	6x6
3	$\mathbf{z} = [\mathbf{B}_m \quad \mathbf{S}_m]^T$	6x6	6x6
4	$\mathbf{z} = [\mathbf{B}_m \quad \mathbf{S}_m \quad \boldsymbol{\omega}_m]^T$	9x6	9x9

References

- [1] M.Y. Ovchinnikov, D.S. Ivanov, Approach to study satellite attitude determination algorithms, *Acta Astronaut.* 98 (2014) 133–137.
- [2] H. Ma, S. Xu, Magnetometer-only attitude and angular velocity filtering estimation for attitude changing spacecraft, *Acta Astronaut.* 102 (2014) 89–102.
doi:<https://doi.org/10.1016/j.actaastro.2014.05.002>.
- [3] Y. Mashtakov, M. Ovchinnikov, F. Wöske, B. Rievers, M. List, Attitude determination & control system design for gravity recovery missions like GRACE, *Acta Astronaut.* 173 (2020) 172–182. doi:[10.1016/j.actaastro.2020.04.019](https://doi.org/10.1016/j.actaastro.2020.04.019).
- [4] D. Ivanov, M. Ovchinnikov, N. Ivlev, S. Karpenko, Analytical study of microsatellite attitude determination algorithms, *Acta Astronaut.* 116 (2015) 339–348.
doi:<https://doi.org/10.1016/j.actaastro.2015.07.001>.
- [5] E. Thébault, C.C. Finlay, C.D. Beggan, P. Alken, E. Al., International Geomagnetic Reference Field: the 12th generation, *Earth, Planets Sp.* 67:69 (2015).
doi:[10.1186/s40623-015-0228-9](https://doi.org/10.1186/s40623-015-0228-9).
- [6] P. Alken, International Geomagnetic Reference Field IGRF-13, *WDC Solid Earth Geophys.* (2019). <https://www.ngdc.noaa.gov/IAGA/vmod/igrf.html> (accessed October 13, 2020).
- [7] N. Olsen, G. Hulot, T.J. Sabaka, Sources of the Geomagnetic Field and the Modern Data That Enable Their Investigation, in: *Handb. Geomathematics*, Springer Berlin Heidelberg, 2010: pp. 105–124. doi:[10.1007/978-3-642-01546-5_5](https://doi.org/10.1007/978-3-642-01546-5_5).
- [8] C. Constable, Earth's Electromagnetic Environment, *Surv. Geophys.* 37 (2016) 27–45.
doi:[10.1007/s10712-015-9351-1](https://doi.org/10.1007/s10712-015-9351-1).
- [9] U.R. Christensen, Planetary Magnetic Fields and Dynamos, in: *Oxford Res. Encycl. Planet. Sci.*, Oxford University Press, 2019.

doi:10.1093/acrefore/9780190647926.013.31.

- [10] E.K.J. Kilpua, A. Balogh, R. von Steiger, Y.D. Liu, Geoeffective Properties of Solar Transients and Stream Interaction Regions, *Space Sci. Rev.* 212 (2017) 1271–1314. doi:10.1007/s11214-017-0411-3.
- [11] M. Mandea, A. Chambodut, Geomagnetic Field Processes and Their Implications for Space Weather, *Surv. Geophys.* 41 (2020) 1611–1627. doi:10.1007/s10712-020-09598-1.
- [12] R. Pirjola, Geomagnetically induced currents during magnetic storms, *IEEE Trans. Plasma Sci.* 28 (2000) 1867–1873. doi:10.1109/27.902215.
- [13] L.J. Zanetti, T.A. Potemra, B.J. Anderson, R.E. Erlandson, D.B. Holland, M.H. Acuña, J. Kappenman, R. Lesher, B. Feero, Ionospheric currents correlated with geomagnetic induced currents; Freja magnetic field measurements and the Sunburst Monitor System, *Geophys. Res. Lett.* 21 (1994) 1867–1870. doi:10.1029/94GL01425@10.1002/(ISSN)1542-7390.GIC15.
- [14] T. Inamori, S. Nakasuka, Application of Magnetic Sensors to Nano and Micro-Satellite Attitude Control Systems, in: Magn. Sensors - Princ. Appl., InTech, 2012. doi:10.5772/34307.
- [15] M.O. Archer, T.S. Horbury, P. Brown, J.P. Eastwood, T.M. Oddy, B.J. Whiteside, J.G. Sample, The MAGIC of CINEMA: first in-flight science results from a miniaturised anisotropic magnetoresistive magnetometer, *Ann. Geophys.* 33 (2015) 725–735. doi:10.5194/angeo-33-725-2015.
- [16] D. Cilden-Guler, Z. Kaymaz, C. Hajiyev, Assessment of Magnetic Storm Effects under Various Magnetometer Noise Levels for Satellite Attitude Estimation, in: 9th Int. Conf. Recent Adv. Sp. Technol., IEEE, 2019: pp. 769–773. doi:10.1109/RAST.2019.8767834.
- [17] T. Inamori, N. Sako, S. Nakasuka, Strategy of Magnetometer Calibration for Nano-

Satellite Missions and In-Orbit Performance, AIAA Guid. Navig. Control Conf. 7598 (2010).

- [18] T. Inamori, R. Hamaguchi, K. Ozawa, P. Saisutjarit, N. Sako, S. Nakasuka, Online Magnetometer Calibration in Consideration of Geomagnetic Anomalies Using Kalman Filters in Nanosatellites and Microsatellites, *J. Aerosp. Eng.* 29 (2016) 04016046. doi:10.1061/(ASCE)AS.1943-5525.0000612.
- [19] G. Shorshi, I.Y. Bar-Itzhack, Satellite autonomous navigation based on magnetic field measurements, *J. Guid. Control. Dyn.* 18 (1995) 843–850. doi:10.2514/3.21468.
- [20] M.E. Hough, Orbit determination with improved covariance fidelity, including sensor measurement biases, *J. Guid. Control. Dyn.* 34 (2011) 903–911. doi:10.2514/1.53053.
- [21] Y. Beaudoin, A. Desbiens, E. Gagnon, R. Landry, Observability of satellite launcher navigation with INS, GPS, attitude sensors and reference trajectory, *Acta Astronaut.* 142 (2018) 277–288. doi:10.1016/j.actaastro.2017.10.038.
- [22] A. Vorobev, V. Pilipenko, Y. Sakharov, V. Selivanov, Statistical relationships between variations of the geomagnetic field, auroral electrojet, and geomagnetically induced currents, *Solar-Terrestrial Phys.* 5 (2019) 35–42. doi:10.12737/stp-51201905.
- [23] R. Tozzi, I. Coco, P. De Michelis, F. Giannattasio, F. Giannattasio, Latitudinal dependence of geomagnetically induced currents during geomagnetic storms, *Ann. Geophys.* 61 (2018) GM448. doi:10.4401/ag-7788.
- [24] A. Viljanen, H. Nevanlinna, K. Pajunpää, A. Pulkkinen, Time derivative of the horizontal geomagnetic field as an activity indicator, *Ann. Geophys.* 19 (2001) 1107–1118. doi:10.5194/angeo-19-1107-2001.
- [25] A. Viljanen, E.I. Tanskanen, A. Pulkkinen, Relation between substorm characteristics and rapid temporal variations of the ground magnetic field, *Ann. Geophys.* 24 (2006) 725–733. doi:10.5194/angeo-24-725-2006.

- [26] E.C. Kalafatoğlu Eyigüler, Z. Kaymaz, Magnetic and electric field variations during geomagnetically active days over Turkey, *Adv. Sp. Res.* 60 (2017) 1921–1948. doi:10.1016/j.asr.2017.07.019.
- [27] B. Fan, Q. Li, T. Liu, How Magnetic Disturbance Influences the Attitude and Heading in Magnetic and Inertial Sensor-Based Orientation Estimation, *Sensors.* 18 (2018). doi:10.3390/s18010076.
- [28] N.A. Matteo, Y.T. Morton, Ionosphere Geomagnetic Field: Comparison of IGRF Model Prediction and Satellite Measurements 1991–2010, *Radio Sci.* 46 (2011). doi:10.1029/2010RS004529.
- [29] D. Cilden-Guler, Z. Kaymaz, C. Hajiyev, Evaluation of Geomagnetic Field Models using Magnetometer Measurements for Satellite Attitude Determination System at Low Earth Orbits: Case Studies, *Adv. Sp. Res.* 61 (2018) 513–529. doi:10.1016/j.asr.2017.10.041.
- [30] D. Cilden, Z. Kaymaz, C. Hajiyev, Extraterrestrial magnetic field effects on attitude determination accuracy of small satellites, in: 7th Int. Conf. Recent Adv. Sp. Technol., IEEE, 2015: pp. 707–711. doi:10.1109/RAST.2015.7208433.
- [31] D. Cilden-Guler, Z. Kaymaz, C. Hajiyev, Geomagnetic Models at Low Earth Orbit and Their Use in Attitude Determination, in: 8th Int. Conf. Recent Adv. Sp. Technol., IEEE, 2017. doi:10.1109/RAST.2017.8003011.
- [32] N.A. Tsyganenko, A Magnetospheric Magnetic Field Model with a Warped Tail Current Sheet, *Planet. Sp. Sci.* 37 (1989) 5.
- [33] N.A. Tsyganenko, Modeling the Earth's Magnetosphere Using Spacecraft Magnetometer Data, (2008). <http://geo.phys.spbu.ru/~tsyganenko/modeling.html>.
- [34] D.H. Fairfield, N.A. Tsyganenko, A. V. Usmanov, M. V. Malkov, A large magnetosphere magnetic field database, *J. Geophys. Res.* 99 (1994) 11319. doi:10.1029/94ja00255.

- [35] C. Hajiyev, D. Cilden Guler, D. Cilden-Guler, Review on Gyroless Attitude Determination Methods for Small Satellites, *Prog. Aerosp. Sci.* 90 (2017) 54–66. doi:10.1016/j.paerosci.2017.03.003.
- [36] J.L. Marins, Xiaoping Yun, E.R. Bachmann, R.B. McGhee, M.J. Zyda, An extended Kalman filter for quaternion-based orientation estimation using MARG sensors, in: *Proc. 2001 IEEE/RSJ Int. Conf. Intell. Robot. Syst. Expand. Soc. Role Robot. Next Millenn. (Cat. No.01CH37180)*, IEEE, n.d.: pp. 2003–2011. doi:10.1109/IROS.2001.976367.
- [37] R.E. Kalman, A New Approach to Linear Filtering and Prediction Problems, *Trans. ASME-Journal Basic Eng.* 82 (1960) 35–45.
<http://www.unitedthc.com/DSP/Kalman1960.pdf>.
- [38] E.P. Babcock, T. Bretl, CubeSat Attitude Determination via Kalman Filtering of Magnetometer and Solar Cell Data, in: *25th Annu. AIAA/USU Conf. Small Satell.*, 2011.
<http://digitalcommons.usu.edu/cgi/viewcontent.cgi?article=1152&context=smallsat> (accessed July 26, 2017).
- [39] B.Y. Mimasu, J.C. Van der Ha, T. Narumi, Attitude determination by magnetometer and gyros during eclipse, in: *AIAA/AAS Astrodyn. Spec. Conf. Exhib.*, American Institute of Aeronautics and Astronautics, Honolulu, USA, 2008. doi:10.2514/6.2008-6932.
- [40] D.A. Vallado, P. Crawford, SGP4 orbit determination, in: *AIAA/AAS Astrodyn. Spec. Conf.*, Code available at: “<http://www.centerforspace.com/downloads/>,” Honolulu, Hawaii, 2008. doi:10.2514/6.2008-6770.
- [41] J.R. Wertz, *Spacecraft Attitude Determination and Control*, D.Reidel Publishing Company, Dordrecht, Holland, 2002.
- [42] C.T. Russel, Geophysical Coordinate Transformations, *Cosm. Electrodyn.* 2 (1971) 184–196.

- [43] N.A. Tsyganenko, Global quantitative models of the geomagnetic field in the cislunar magnetosphere for different disturbance levels, *Planet. Space Sci.* 35 (1987) 1347–1358. doi:10.1016/0032-0633(87)90046-8.
- [44] N.A. Tsyganenko, Quantitative models of the magnetospheric magnetic field: Methods and results - A review, *Space Sci. Rev.* 54 (1990) 75–186. doi:10.1007/BF00168021.
- [45] N.A. Tsyganenko, A global analytical representation of the magnetic field produced by the region 2 Birkeland currents and the partial ring current, *J. Geophys. Res. Sp. Phys.* 98 (1993) 5677–5690. doi:10.1029/92ja02002.
- [46] N.A. Tsyganenko, Modeling the Earth's Magnetospheric Magnetic Field Confined within a Realistic Magnetopause, *J. Geophys. Res.* 100 (1995) 5599–5612.
- [47] N.A. Tsyganenko, A model of the near magnetosphere with a dawn-dusk asymmetry 1. Mathematical structure, *J. Geophys. Res. Sp. Phys.* 107 (2002) SMP 12-1-SMP 12-15. doi:10.1029/2001JA000219.
- [48] Planetary K-index | NOAA / NWS Space Weather Prediction Center, (n.d.). <https://www.swpc.noaa.gov/products/planetary-k-index> (accessed October 13, 2020).
- [49] Kp Index, (n.d.). <https://www.gfz-potsdam.de/en/kp-index/> (accessed November 3, 2020).
- [50] M. Siebert, J. Meyer, Geomagnetic Activity Indices, in: W. Dieminger, G.K. Hartmann, R. Leitinger (Eds.), Up. Atmos., Springer Berlin Heidelberg, 1996: pp. 887–911. doi:10.1007/978-3-642-78717-1_26.
- [51] Geomagnetic Kp and Ap Indices | NCEI, (n.d.). https://www.ngdc.noaa.gov/stp/GEOMAG/kp_ap.html (accessed October 13, 2020).
- [52] D.A. Vallado, Fundamentals of Astrodynamics and Applications (3rd Ed.), Microcosm Press/Springer, USA, 2007.
- [53] H.E. Soken, C. Hajiye, S. Sakai, Robust Kalman Filtering for Small Satellite Attitude

Estimation in the Presence of Measurement Faults, *Eur. J. Control.* 20 (2014) 64–72.

doi:10.1016/j.ejcon.2013.12.002.

- [54] C. Hajiye, D. Cilden, Y. Somov, Gyro-free attitude and rate estimation for a small satellite using SVD and EKF, *Aerospace Sci. Technol.* 55 (2016) 324–331.
doi:10.1016/j.ast.2016.06.004.

- [55] R. DaForno, F. Reali, S. Bristor, S. Debei, Autonomous Navigation of MegSat1: Attitude, Sensor Bias and Scale Factor Estimation by EKF and Magnetometer-Only Measurement, in: 22nd AIAA Int. Commun. Satell. Syst. Conf. Exhib., California, USA, 2004. doi:10.2514/6.2004-3183.



Demet Cilden-Guler received her BSc and MSc from Istanbul Technical University in 2014, and 2016 respectively. She is currently a PhD candidate at Aeronautical and Astronautical Engineering Department, Istanbul Technical University. She is the author/coauthor of 30 conference and 9 SCI journal papers. She is supported by ASELSAN (Military Electronic Industries) and TUBITAK (Scientific and Technological Research Council of Turkey) PhD Scholarships. She is one of the 2018 Amelia Earhart Fellows. Her professional interest areas are Kalman filtering, attitude determination and control of small satellites, extraterrestrial magnetic field and planets' albedo effects on satellite's attitude, and integrated estimation methods.



Zerefsan Kaymaz currently works as a full professor at İstanbul Technical University, Faculty of Aeronautics and Astronautics. She received her PhD from Department of Atmospheric Sciences at UCLA. She studied as a researcher in Boston University, Max Planck Institute for Aeronomy, APL, and NASA/GSFC Space Weather Laboratory. She received Alexander von Humboldt fellowship, and TÜBİTAK Young Scientist award in Upper Atmosphere and Space Physics in Turkey. Her research is focused on Space Environment and its effects on Satellites. She acts as a referee in international journals and evaluator in European Union projects. She is a member of AGU, COSPAR, IAA.



Chingiz Hajiyev graduated from Moscow Aviation Institute, Moscow, Russia, with honors in 1981. He received his Ph.D. and DSc(Eng) degrees in Process Control in 1987 and 1993, respectively. He joined to Department of Aeronautical Engineering, Istanbul Technical University, Turkey in 1996 as a Professor. Since December 2016, he is also the head of the Aeronautical Engineering Department. He is the author about 500 scientific publications

including 14 books, 18 book chapters and more than 300 international journal and international conference papers. His research interests include attitude determination and control, fault diagnosis, fault tolerant control, Kalman filtering and integrated navigation systems.